



Dielectric relaxations and optical properties of Mn-doped ZnO nanoparticles

T. Abdel-Baset^{1,2}, S. Saber¹, and S. El-Sayed^{1,*}

¹Department of Physics, Faculty of Science, Fayoum University, El Fayoum 63514, Egypt

²Department of Physics, Faculty of Science, Taibah University, Yanbu 46423, Saudi Arabia

Received: 27 July 2020

Accepted: 4 October 2020

Published online:
15 October 2020

© Springer Science+Business
Media, LLC, part of Springer
Nature 2020

ABSTRACT

Nanoparticles (NPs) of pure zinc oxide (ZnO) and $Zn_{1-x}Mn_xO$, where $x = 0.01$ and 0.05 , were prepared using the co-precipitation method. The X-ray diffraction patterns revealed that both pure ZnO and Mn-doped ZnO NPs crystallize in hexagonal wurtzite. Different structure parameters are given. Other characterizations, such as scanning electron microscopy, energy-dispersive X-ray spectroscopy, and FTIR, were used to test the studied samples. The dielectric and optical properties were performed and discussed in detail. It was found that the dielectric permittivity and the ac conductivity of pure ZnO NPs increased significantly when the Mn ions substituted the Zn ones. A small polaron hopping conduction mechanism is suggested for the investigated samples. Different optical parameters were calculated in this work. The outcome results are discussed and compared to similar materials.

1 Introduction

Zinc oxide (ZnO) is one of the most promising materials for different applications such as solar cells, light emitter, and optical sensors. [1, 2]. Therefore, ZnO has great attention owing to its direct bandgap (≈ 3.37 eV) and binding energy (60 meV). With these features, ZnO is still an active area of research.

There are different and numerous publications on transition metal-doped ZnO [3–15] since it is an interesting subject of research. It was found that the physical properties of ZnO depend on the type of the transition metals which substituted Zn. For instance, the optical bandgap, E_g , dielectric constant, and magnetic properties of ZnO increased as the content

of Co in $Zn_{1-x}Co_xO$ increased [3–5]. Both optical and magnetic properties of ZnO were improved by the doping of Fe ions [6], where the crystal structure did not change up to 5 wt% of Fe while a ferromagnetic transition around the room temperature (RT) was observed. Furthermore, a higher photocatalytic activity, as well as a decrease in E_g , was reported for Mg-doped ZnO [7].

Different groups have been focused on the physical properties of Mn-doped ZnO [8–15]. The outcome results can be summarized as; the physical properties of ZnO depend on the content of Mn ions, the crystal structure is hexagonal wurtzite [8, 9], the conduction mechanism is hopping [10], the dielectric constant and electrical conductivity were enhanced [11], a

Address correspondence to E-mail: ssa06@fayoum.edu.eg

magnetic transition was observed at RT [8], the E_g is blueshifted compared with that of pure ZnO [12], the combination of Mn-doped ZnO with poly(3-hexythiophene) is good for solar energy [13], there is a clear change in the transmittance around 400 nm [14], and finally an interesting variation of the E_g was observed when Mn-doped ZnO [15].

Mote et al. [16] reported on the structure, morphology, and optical properties of $Zn_{1-x}Mn_xO$ nanoparticles (NPs), where $0 \leq x \leq 0.20$. The results showed that the structure is still wurtzite (hexagonal). With the increase in the content of Mn, the lattice parameters and the packing fraction increased in contrast with the optical bandgap. Moreover, the optical properties of ZnO nanosized doped with different ions such as Cd, Mg, Mn, and Fe were studied [17]. It was found that the E_g can be changed from 2.9 to 3.8 eV dependent on the type of the dopants. Moreover, the electrical conductivity of Al- and Mn-doped ZnO is semiconducting-like and depends on the sintering temperature as well as the type of doping ions [18].

For all previous studies, the effect of the transition metals on the physical features of the ZnO NPs is still a very active area of research because of its interesting dielectric, optical, and magnetic properties. The dielectric properties are essential for examining the relaxation processes and conduction mechanisms in semiconducting-like materials. Besides, they are important in the electronic industry and engineers when the studied dielectrics come to be capacitor performance, antennas, or substrates. From our knowledge, there are no detailed studies of the dielectric spectroscopy of Mn-doped ZnO nanoparticles, especially at the content of 1 and 5 wt% Mn ions. Therefore and after characterizing the synthesized samples, this work targeted to analyze the dielectric properties of Mn-doped ZnO NPs in addition to give different important optical parameters.

2 Experimental

2.1 Synthesis of $Zn_{1-x}Mn_xO$ NPs

$Zn_{1-x}Mn_xO$ NPs, where $x = 0, 0.01, \text{ and } 0.05$, have been prepared. $ZnSO_4$ and NaOH solutions were mixed together. The solution was preserved at room temperature (RT) with 2 h continuous stirring. Then, it was heated at 70 °C for 24 h for drying. The dried

product was sintered at 400 °C for 4 h and left to cool down slowly to RT to get pure ZnO. In order to prepare the mixed oxide samples, both $ZnSO_4$ and $MnSO_4$ solutions were mixed at the desired ratio. NaOH solution is added gradually to the mixed solution. Similar processes, as described for the as-prepared ZnO, were considered to obtain $Zn_{1-x}Mn_xO$ nanoparticles.

2.2 Characterization techniques

X-ray diffraction (XRD) of the investigated samples is studied using a Rigaku diffractometer with Cu K_{α} radiation ($\lambda = 1.5406 \text{ \AA}$). The morphologies of the synthesized samples were done using a field emission scanning electron microscope, FE-SEM (LEO SUPRA 55VP FEG, Zeiss, equipped with Oxford EDX detector). FTIR spectra are obtained using a Shimadzu 8201 PC in (400–4000 cm^{-1}) range. Dielectric measurements were performed over a wide range of frequencies using a Hioki (Ueda, Nagano, Japan) model 3532 High Tester LCR. The dielectric constant (ϵ') and losses (ϵ'') were calculated:

$$\epsilon' = \frac{Cd}{\epsilon_0 A}, \quad \epsilon'' = \epsilon' \tan \delta, \quad (1)$$

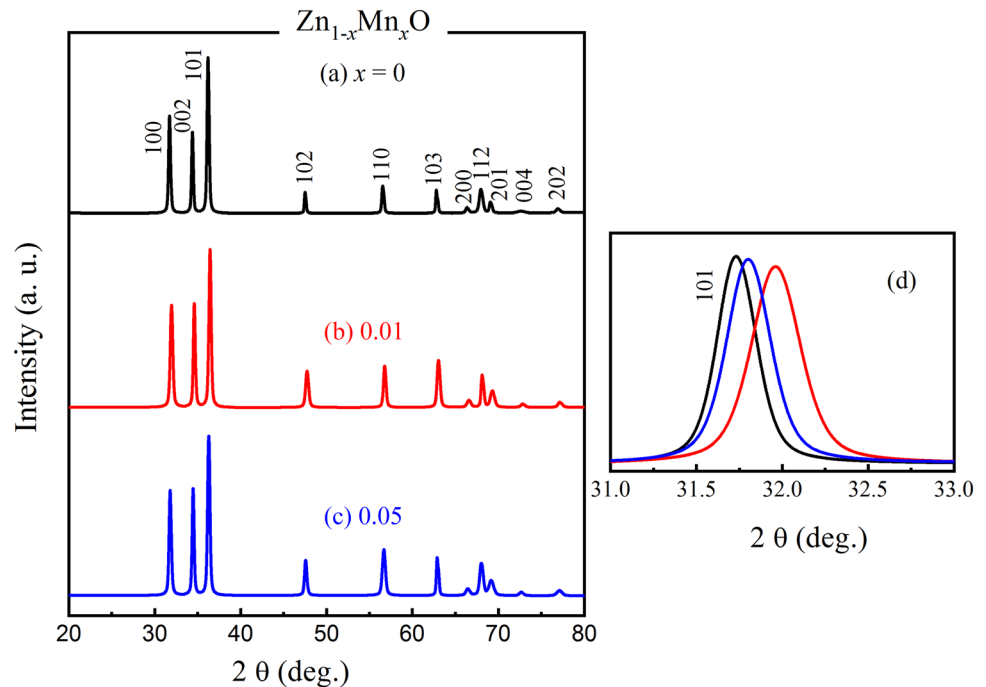
where C is the capacitance, ϵ_0 is the permittivity of vacuum, $\tan \delta$ is the loss tangent. A and d are the cross-sectional area and the thickness of the sample, respectively. Optical measurements were performed at room temperature using a Shimadzu UV-3600 UV-Vis-NIR spectrophotometer in the wavelength (200–900 nm) range.

3 Results and discussion

3.1 Characterizations

Figure 1a–d depict the XRD patterns of the $Zn_{1-x}Mn_xO$ NPs, which revealed that pure ZnO and Mn-doped ZnO NPs are single-phase and crystallize in hexagonal (wurtzite) similar to previous reports [8, 9, 16, 19]. The lattice constants with the unit cell volume are given in Table 1. The lattice parameters of the studied samples are matched well with earlier reports for pure ZnO Nps [3, 6, 16, 20, 21] as well as for Mn-doped ZnO NPs [16, 20, 21]. The crystal parameters are slightly changed when Mn substituted Zn ion due to the difference in the ionic radii of

Fig. 1 a–d The XRD patterns of the $\text{Zn}_{1-x}\text{Mn}_x\text{O}$ NPs, where $x = 0, 0.01$ and 0.05



these two ions [16]. More evidence is Fig. 1d, where a shift of the main diffraction peak to higher 2θ is observed for Mn-doped ZnNPs. Besides, the shift of 2θ for the sample of $x = 0.01$ is more clear than that of $x = 0.05$. This shift was also reported for Fe-doped ZnO NPs [22]. The bond lengths were also calculated using Eq. 2 [23, 24] and listed in Table 1.

$$l = \sqrt{\left(\frac{a^2}{3} + \left(\frac{1}{2} - u\right)^2 c^2\right)} \quad (2)$$

where c and a are the lattice constants. The positional or internal parameter in the wurtzite hexagonal structure (u) was determined as:

$$u = \frac{a^2}{3c^2} + \frac{1}{4} \quad (3)$$

The values of the bond lengths of Zn–O/Mn–O reflect our argument that the Mn ions substituted

well the Zn ones and are consistent with the previous reports [24].

The average grain size (D_{av}) of the investigated samples was obtained from the XRD patterns using Scherrer's formula:

$$D = 0.9\lambda / (B \cos \theta), \quad (4)$$

where θ is Bragg's angle, $\lambda \approx 1.54 \text{ \AA}$, and B is the FWHM (the full width at half maximum). The values of the D_{av} are given in Table 1. The values of D_{av} are consistent with the earlier report [9]. In addition, the lattice strains (β) were calculated [7, 25, 26]:

$$\beta = \frac{B}{4 \tan \theta} \quad (5)$$

The average values of β are given in Table 1. The sample of $x = 0.01$ has smaller value of β than those of $x = 0$ and 0.05 .

The FE-SEM images of $\text{Zn}_{1-x}\text{Mn}_x\text{O}$ NPs are presented in Fig. 2a–c. The average crystal sizes are

Table 1 The lattice parameters, the unit cell volume (V), the positional parameter (u), the bond length (l), the average crystal size (D_{av}), and the average lattice strain (β) for both pure ZnO and Mn-doped ZnO NPs

x	a (Å)	c (Å)	V (Å ³)	u	l (Å)	D_{av} (nm)	$\beta \times 10^{-2}$
0	3.249	5.203	54.923	0.3799	1.977	43.7	0.24
0.01	3.248	5.204	54.899	0.3798	1.977	40.0	0.23
0.05	3.250	5.206	54.988	0.3799	1.978	31.5	0.29

about 39.75, 35.82, and 29.52 nm for the samples of $x = 0, 0.01, \text{ and } 0.05$, respectively. As seen, the crystal sizes of both ZnO and Mn-doped ZnO NPs are almost consistent with those calculated using XRD patterns (see Table 1). The shape of the particle size is similar to that published by Shatnawi et al. [20]. The EDX spectra of all studied samples are displayed in Fig. 2d–f. It was found that the estimated element compositions (see the inserted Table for each sample) are in good agreement with the used components for each synthesized NPs. The EDX spectrum and element compositions of this work matched well to the earlier reports either for pure ZnO [27] or Mn-doped ZnO NPs [28, 29]. This confirms the purity of the prepared samples.

The FTIR spectra are displayed in Fig. 3. The main FTIR peaks are their locations shown by the arrows in this figure. All wavenumbers and their assignments are summarized in Table 2. The observed peaks of the

as-prepared ZnO NPs are consistent with earlier reports [30–33] and similar to those observed in the as-prepared NiO₂ NPs [34]. Through doping, some peak position of the ZnO bands was slightly altered, especially around 555 cm⁻¹ because of the metal oxide vibration [33]. Also, the peak around 1626 cm⁻¹ is due to Zn–O stretching vibration [24]. This means that the substitution of Zn by Mn slightly interrupted the ZnO lattice. The same results were reported for Ni-doped ZnO NPs [35].

3.2 Dielectric properties

3.2.1 Frequency dependence

Figure 4a–d depict the frequency-dependent dielectric permittivity (ϵ') of the investigated samples at different temperatures. The normal behavior of the ϵ' versus frequency with increasing temperature is

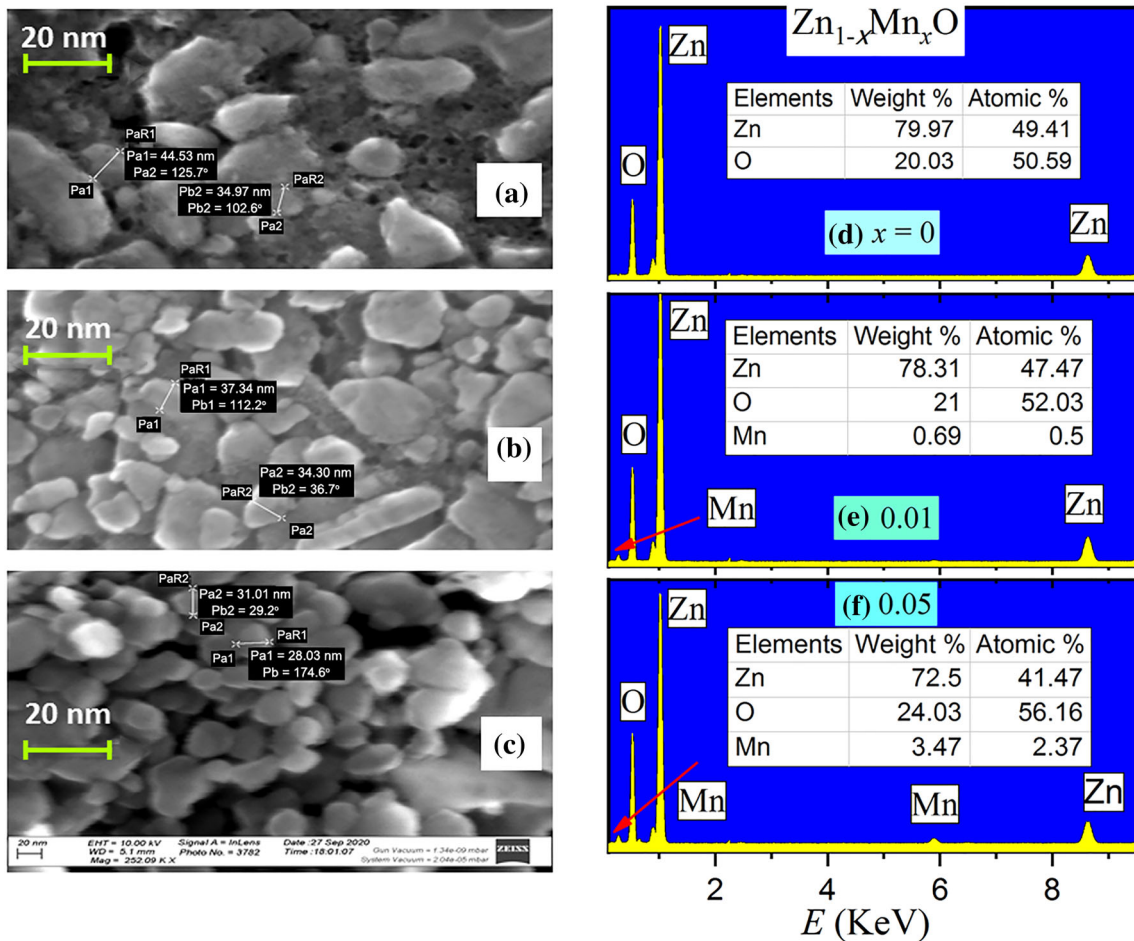


Fig. 2 a–c The FE-SEM images of the Zn_{1-x}Mn_xO NPs, where $x = 0$ (a), 0.01 (b), 0.05 (c). d–f the EDX spectra of the investigated samples

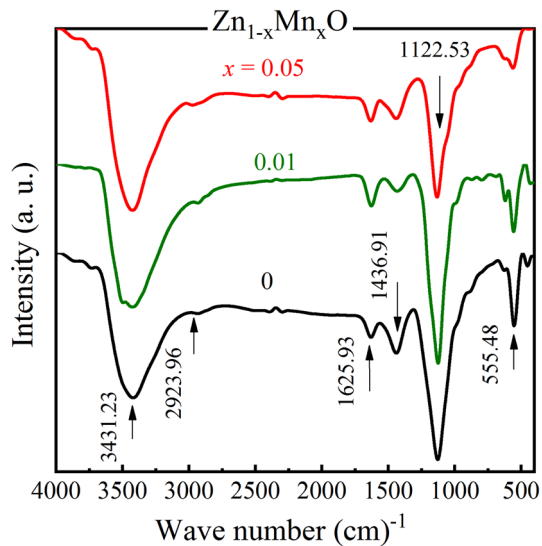


Fig. 3 The FTIR spectra of pure ZnO and Mn-doped ZnO NPs. The arrows guide the eyes to the position of the main peaks to show the difference between undoped and doped samples

observed and consistent with the previously reported for pure ZnO NPs [36] and for $\text{Zn}_{0.94}\text{Mn}_{0.06}\text{O}$ [14]. Interesting is the pronounced increase in the values

Table 2 The main FTIR peaks and their assignments [20, 23, 27, 28] for pure ZnO and Mn-doped ZnO NPs

Wavenumber (cm^{-1})	Assignments
555.48	M–O metal oxide stretching vibration
1122.53	C–O asymmetric stretching
1625.93	Zn–O stretching vibration
2923.96	C–H stretching vibration
3431.23	O–H stretching vibration

of ϵ' for pure ZnO NPs when the Mn ion substituted Zn one. This result could be attributed to the interfacial polarization, as well as the probability of the existence of a mixture of different oxidation of states of Mn ions as $\text{Mn}^{2+}/\text{Mn}^{3+}$. It is noticed that the sample of $x = 0.01$ showed a higher value of ϵ' than those of $x = 0$ and 0.05.

The frequency-dependent dielectric losses (ϵ'') of pure ZnO and Mn-doped ZnO NPs at some selected temperatures are presented in Fig. 5a–c. Again, the typical behavior of the ϵ'' has been recognized for all investigated samples similar to the earlier reports for

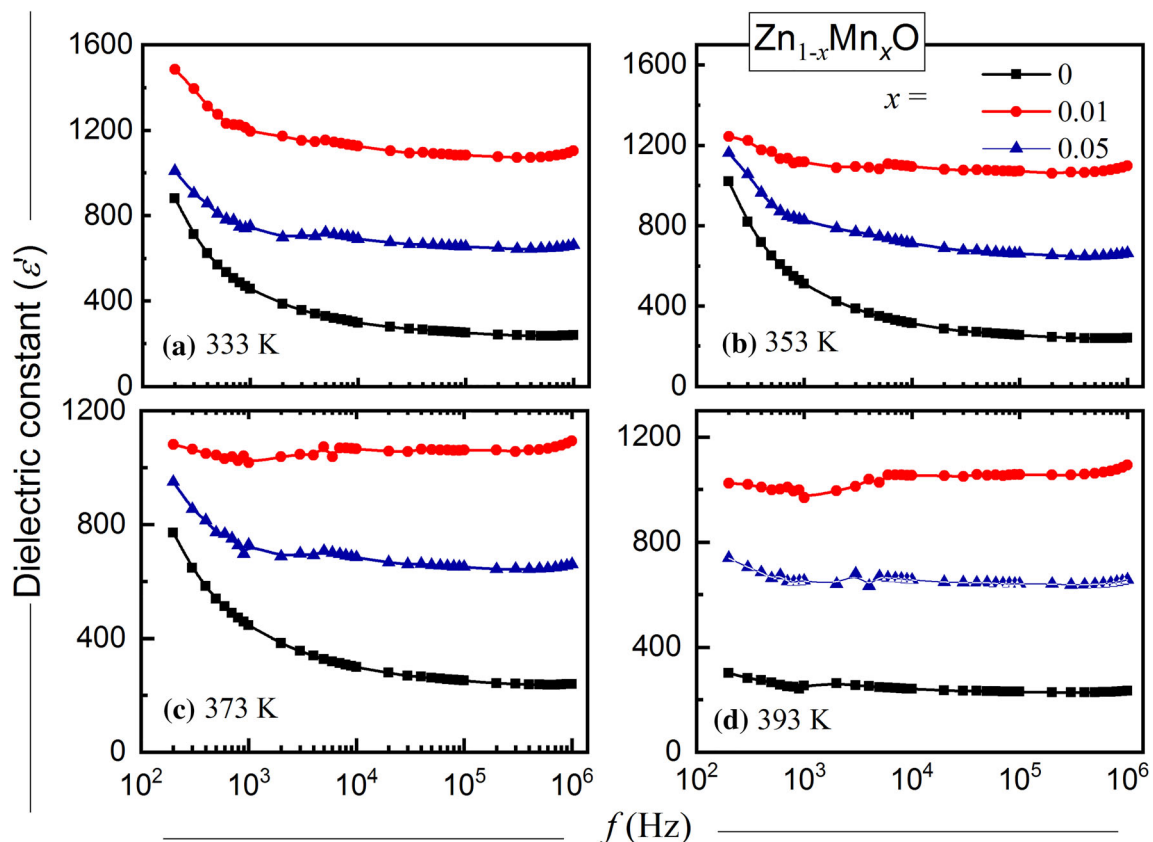


Fig. 4 a–d The $\epsilon'(f)$ curves of the studied samples at different temperatures

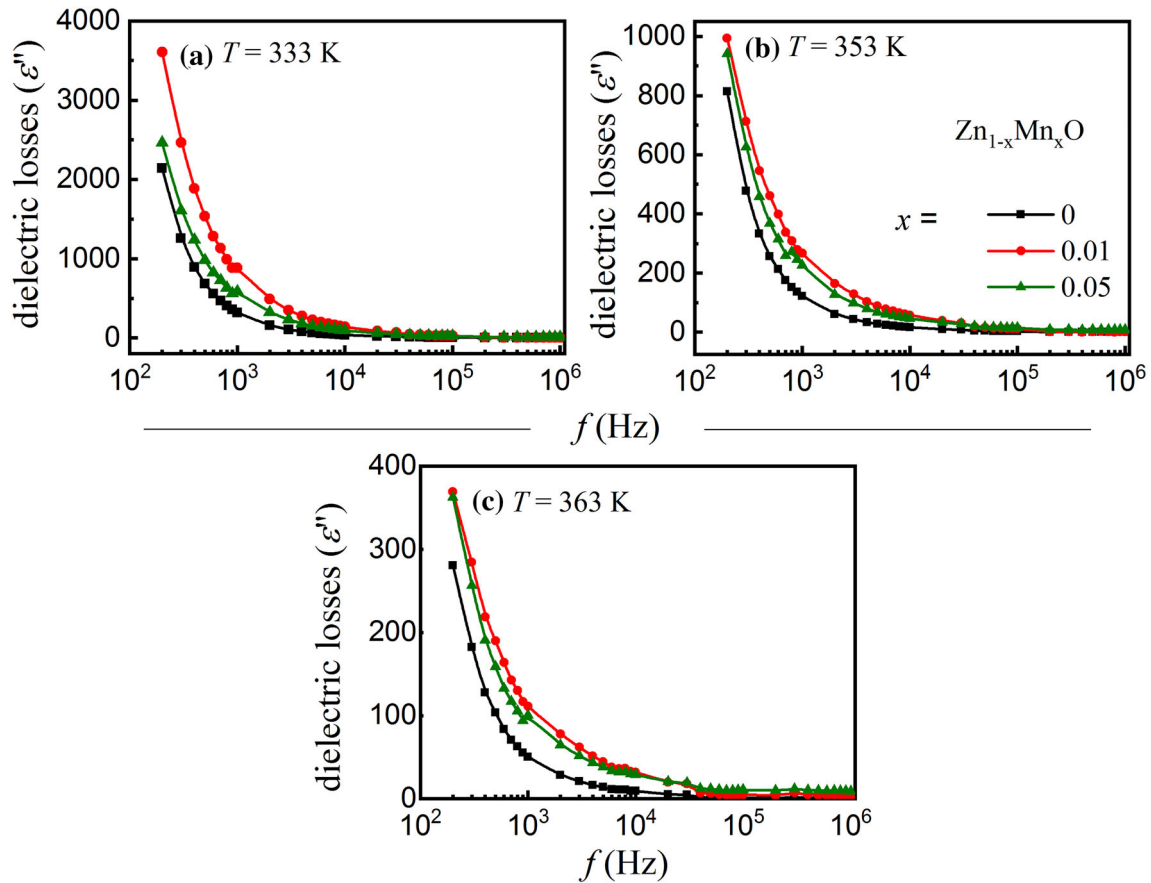


Fig. 5 a–c The $\epsilon''(f)$ curves for pure ZnO and Mn-doped ZnO NPs at different temperatures, for instance

pure ZnO NPs [37] and for $\text{Zn}_{0.94}\text{Mn}_{0.06}\text{O}$ [14]. Besides, the losses at low frequencies of pure ZnO NPs increased with the substituting of Zn by Mn ions.

The frequency dependence of the σ_{ac} of pure ZnO and Mn-doped ZnO NPs at some selected temperatures are displayed in Fig. 6a–d. As seen, the σ_{ac} of all studied samples increased with increased frequency. The $\sigma_{ac}(f)$ data were fitted using this formula [38, 39]:

$$\sigma_{ac}(f) = \sigma_t - \sigma_{dc} \approx 2\pi Af^s \tag{6}$$

where σ_t is the total ac conductivity, σ_{dc} is the low-frequency conductivity, A is a factor, while s is the frequency exponent parameter. The σ_{ac} of pure ZnO increased when Mn substituted Zn ion, and the sample of $x = 0.01$ showed the highest values of the Ac conductivity compared to the others. The values of the s were obtained from the slopes of the lines in Fig. 6a–d, and given in Table 3. It is observed that the values of s increased with increasing temperature up to 393 K and then decreased with increasing T except for $x = 0.05$. A different trend is noticed for the values

of $\log(A)$ (see Table 3). Since the value of s ($0 \leq s \leq 1$) increased with temperature ($333 \text{ K} \leq T \leq 393 \text{ K}$), then the conduction mechanism can be attributed to a small polaron hopping type. A similar suggestion was reported to lead-free perovskite ceramics [40].

3.2.2 Temperature dependence

The temperature dependence of the ϵ' of pure ZnO and Mn-doped ZnO NPs are shown in Fig. 7a–d. As seen, the ϵ' of pure ZnO is remarkably increased with increasing the doping of Mn ions. Again, the sample of $x = 0.01$ exhibited the highest values of ϵ' compared to those of $x = 0$ and 0.05. At $f \leq 0.4 \text{ kHz}$, the $\epsilon'(T)$ of $x = 0$ and 0.05 showed a peak of around 345 K. On the other hand, the $\epsilon'(T)$ of the sample of $x = 0.01$ exhibited the same peak around 330 K. With increasing f , such a peak became broad at 3 kHz and disappeared when $f > 3 \text{ kHz}$. Different reasons could be possible for the existence of such a peak in $\epsilon'(T)$ such as magnetic transitions around room

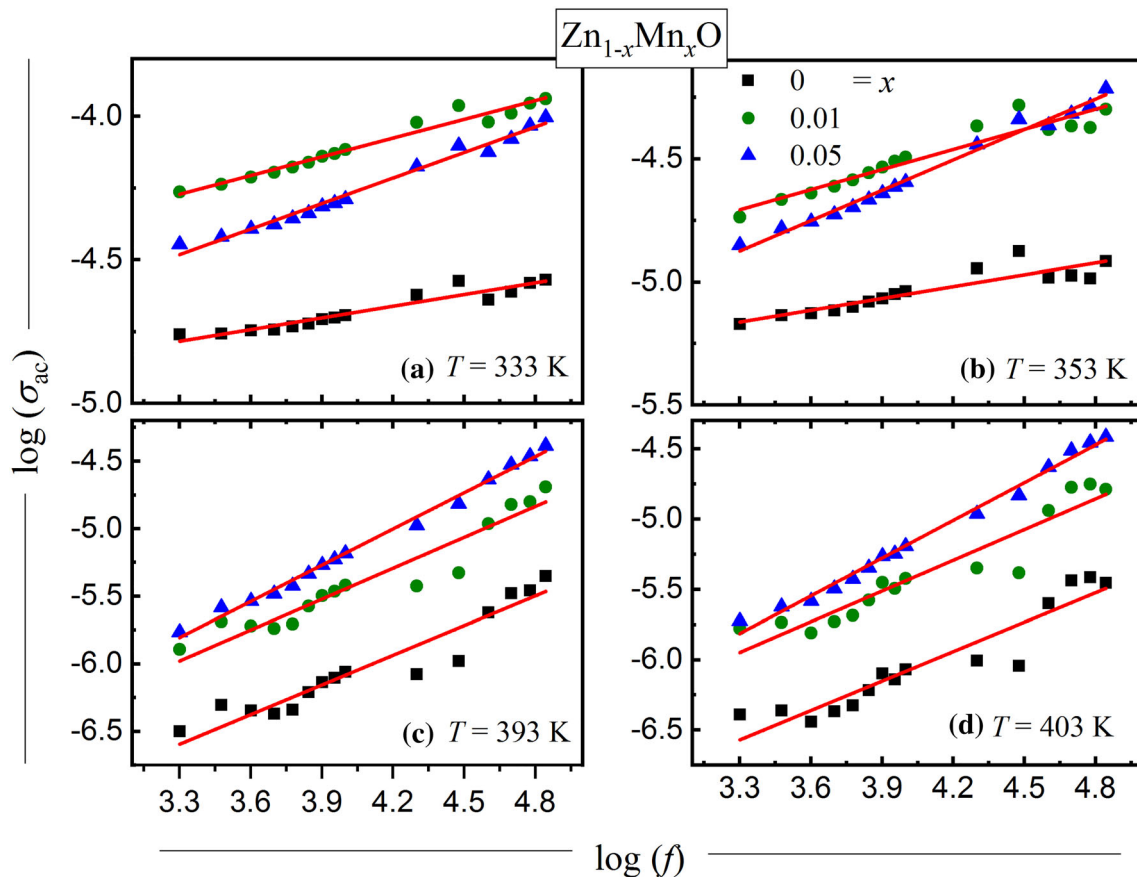


Fig. 6 a–d The frequency-dependent σ_{ac} for pure ZnO and Mn-doped ZnO NPs. The red lines represent the fitting based on Eq. 6 (Color figure online)

Table 3 The frequency exponent, s , and the constant, A , of pure ZnO and Mn-doped ZnO NPs at different temperatures according to the fitting of Eq. 6

Samples	333 K		353 K		393 K		403 K	
	s	$\log(A)$	s	$\log(A)$	s	$\log(A)$	s	$\log(A)$
Pure ZnO	0.136	− 5.462	0.160	− 5.692	0.723	− 9.014	0.698	− 8.875
1.0 wt.% Mn	0.218	− 4.891	0.273	− 5.608	0.893	− 8.756	0.728	− 8.353
5.0 wt.% Mn	0.297	− 5.232	0.412	− 6.234	0.762	− 8.496	0.894	− 8.767

temperature [41] or the resonance response of the orientation dipoles [42].

Figure 8a–f represent the variation of the ε'' versus temperature of pure ZnO and Mn-doped ZnO NPs at different frequencies. All studied samples exhibited a relaxation peak of around 330 K. While the peak position is almost the same for all compounds, the peak height is slightly changed either by increasing the level of doping or the frequency. The temperature dependence of the σ_{ac} of pure ZnO, as well as Mn-doped ZnO NPs at different frequencies, are shown in Fig. 9a–f. As observed, the $\sigma_{ac}(T)$ increased with increasing temperature passing through a maximum

of around 330 K, similar to that observed in the $\varepsilon''(T)$ curves. This relaxation process was also reported for pure ZnO NPs [36]. The sample of $x = 0.01$ showed the highest values of σ_{ac} compared to those of the $x = 0$ and 0.05, as recognized in both ε' and ε'' .

3.3 Optical properties

It is known that the UV–vis spectroscopy is useful to test the optical properties of the materials. Both absorbance (a) and transmittance (T) spectra of pure ZnO and Mn-doped ZnO NPs are depicted in Fig. 9a, b. As seen in Fig. 10a, the $a(\lambda)$ of pure ZnO NPs

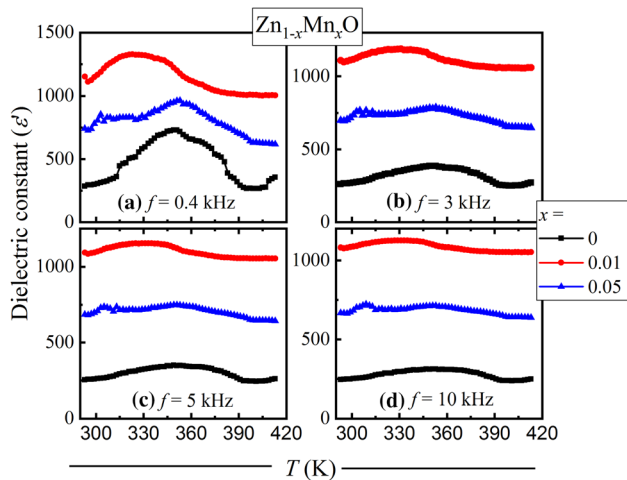


Fig. 7 a–d The $\epsilon'(T)$ plots of $\text{Zn}_{1-x}\text{Mn}_x\text{O}$ NPs, where $x = 0, 0.01$ and 0.05 at different frequencies

decreased in dissimilarity to $T(\lambda)$ (see Fig. 10b) when Zn ion is substituted by Mn one. A transition was seen around 375 nm (≈ 3.31 eV) consistent with the previous reports for pure or M -doped ZnO, where M is Co [4, 43], Mg [7], Ni [12], and Mn [12, 15, 16, 30]. The color shift depends slightly on both M type and its concentration. Furthermore, such a transition could be attributed to the increased concentration of the charge carriers at this absorbed energy.

It is useful to determine the optical energy bandgap (E_g) for the studied samples using this formula [44, 45]:

$$(\alpha h\nu)^2 = \gamma(h\nu - E_g), \tag{7}$$

where γ constant and h Planck's constant. The plot of $(\alpha h\nu)^2$ against $h\nu$ allows us to obtain the values of the

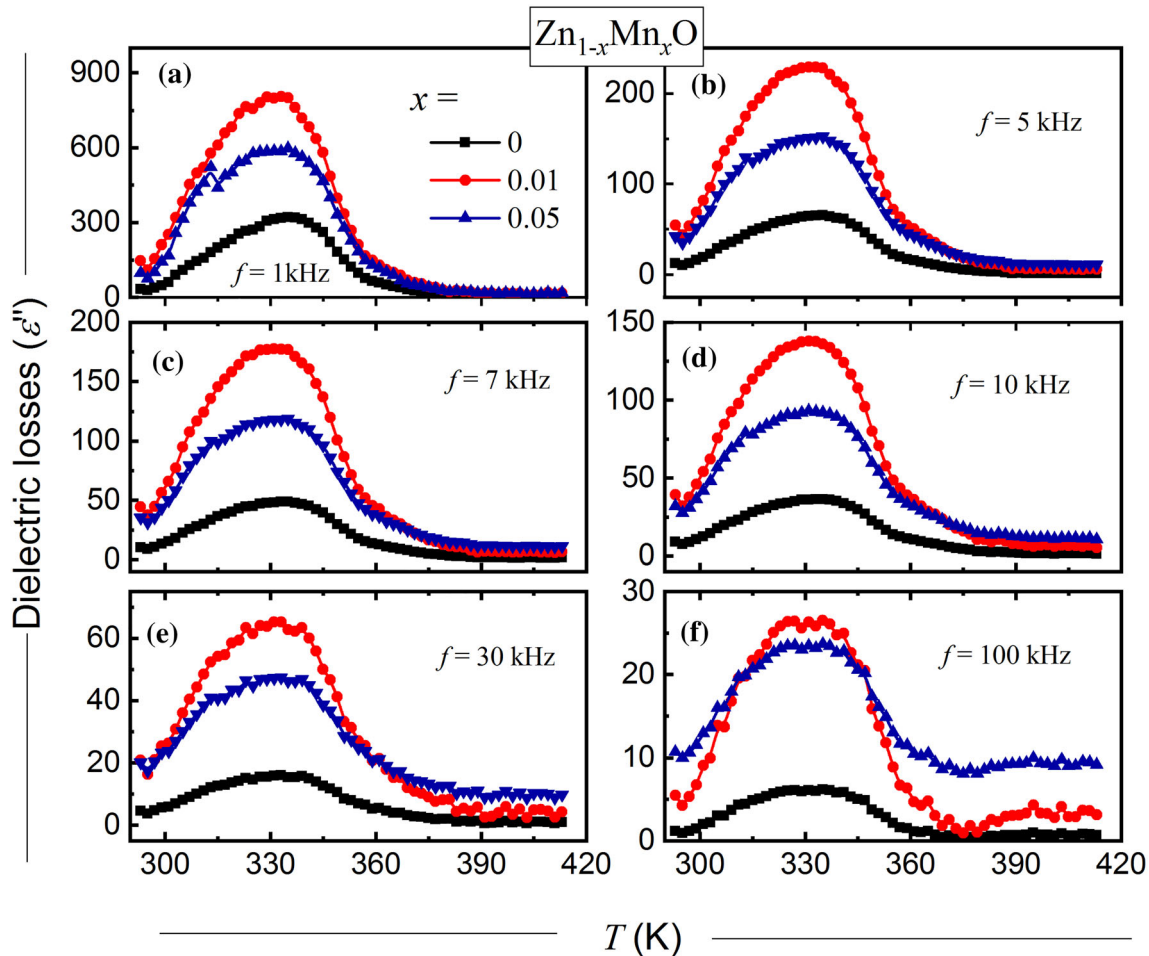


Fig. 8 a–f The $\epsilon''(T)$ plots of $\text{Zn}_{1-x}\text{Mn}_x\text{O}$ NPs, where $x = 0, 0.01$ and 0.05 at different frequencies

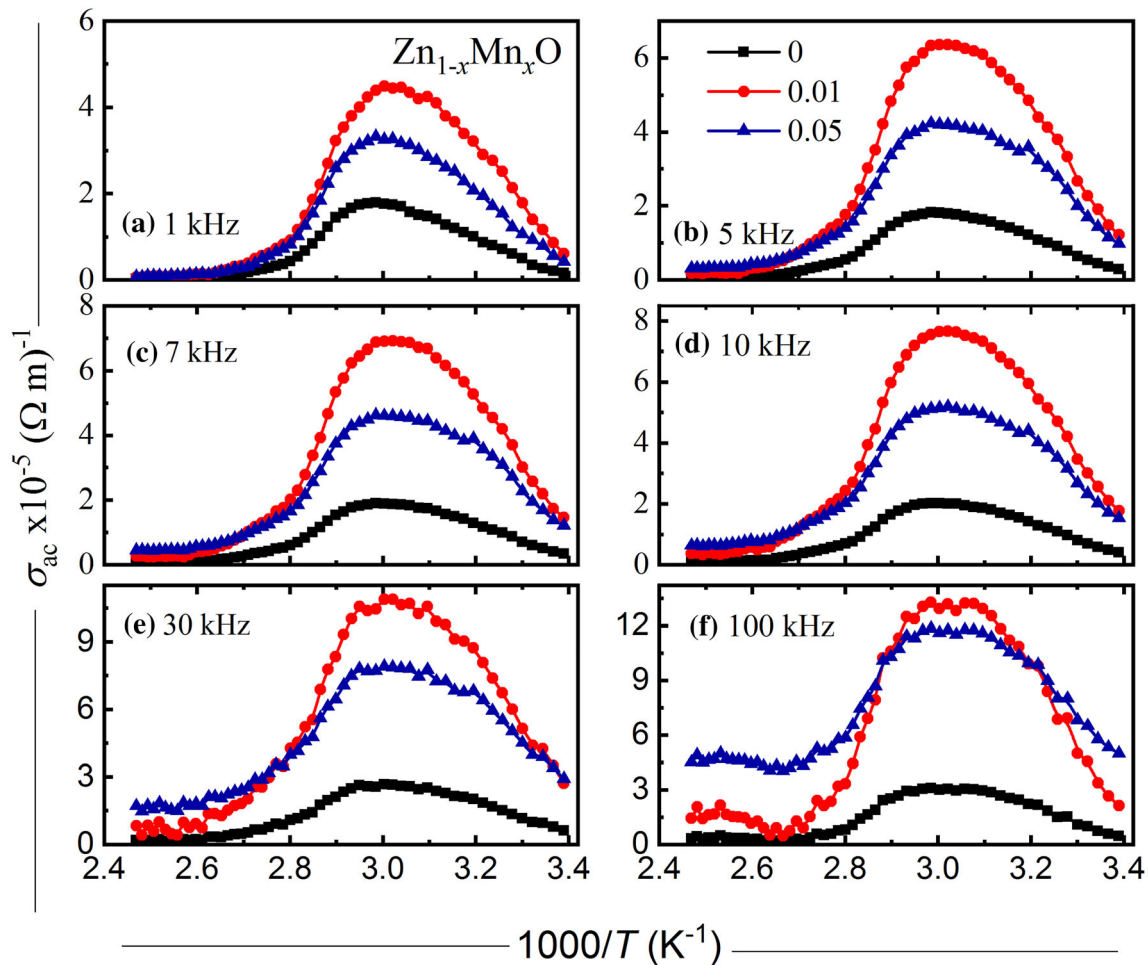


Fig. 9 a–f The temperature dependence of the σ_{ac} for pure ZnO and Mn-doped ZnO NPs at different frequencies

direct E_g as depicted in Fig. 11. The values of E_g are given in Table 4. Figure 12 represents the variation of the absorption coefficient, $\ln(\alpha)$, against the energy, $h\nu$, based on Urbach relation [46]:

$$\ln(\alpha) = \ln(\alpha_0) + (h\nu - r)/E_U \quad (8)$$

where E_U is Urbach energy, r and α_0 are constants. The values of E_U were obtained from the slopes of the straight lines and listed in Table 4. The decrease in E_U with the doping of Mn may reflect the redistribution of optical states allowing a large number of possible transition states.

The refractive index (n) was estimated using the equation [47]:

$$n = \left[4R/(1-R)^2 - k^2 \right]^{1/2} + [(1+R)/(1-R)] \quad (9)$$

where R is the reflectance ($R = 1 - \sqrt{T * \exp(a)}$) [48], and k is the extinction coefficient ($k = \alpha\lambda/4\pi$), λ is the

wavelength. The n dependence of λ for both pure ZnO and Mn-doped ZnO NPs are plotted in Fig. 13a. The values of n decreased with increasing λ . Furthermore, the values of n for pure ZnO NPs decreased with the doping of Mn. The data of $n(\lambda)$ for the investigated samples exhibited an anomalous dispersion around 375 nm (≈ 3.31 eV). Similar anomalous dispersion in the $n(\lambda)$ was observed for pure ZnO [48–51] and Mn-doped ZnO, where M is Ni [39], and Al_2O_3 [51].

Various dispersion parameters could be estimated [52]:

$$\frac{n_\infty^2 - 1}{n^2 - 1} = 1 - \left(\frac{\lambda_0}{\lambda} \right)^2, \quad (10)$$

where λ_0 is the interband oscillating wavelength, n_∞ is the refractive index at long-wavelength. The average oscillator strength (S_0) is related to these parameters (n_∞ , λ_0) as:

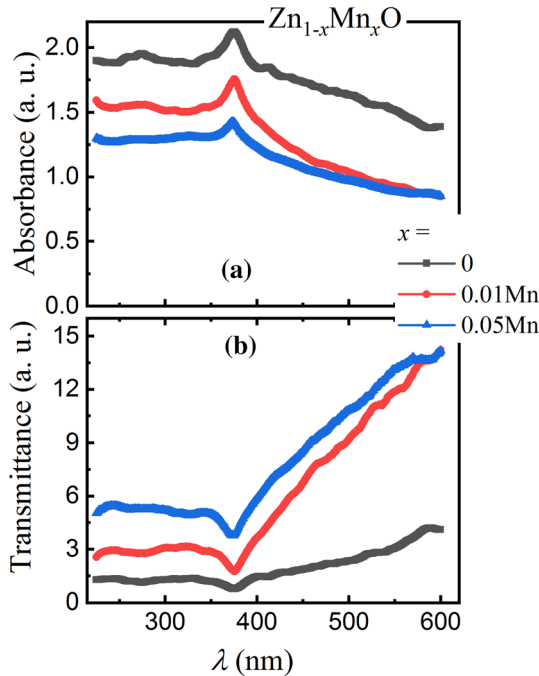


Fig. 10 **a** The absorbance of the UV–vis versus the wavelength (λ). **b** The change of the transmittance (T) with λ for pure ZnO and Mn-doped ZnO NPs

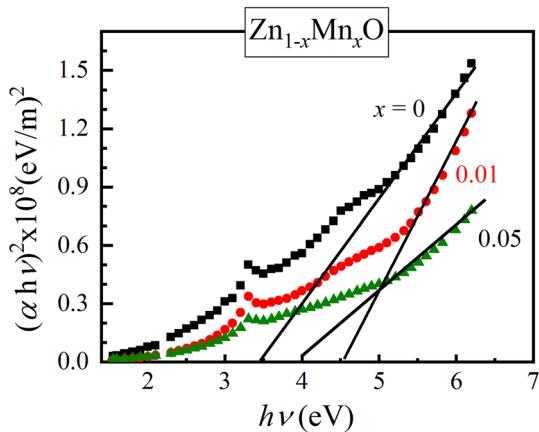


Fig. 11 The variation of $(\alpha h\nu)^2$ against the radiation energy ($h\nu$) for pure ZnO and Mn-doped ZnO NPs

$$S_o = \lambda_o^{-2}(n_\infty^2 - 1) \tag{11}$$

Using the slopes and the intercepts of the plots $(n^2 - 1)^{-1}$ versus λ^{-2} (see Fig. 13b), the parameters n_∞ , λ_o , and then S_o are obtained and tabulated in Table 4. The optical parameters of pure ZnO and Mn-doped ZnO NPs were changed by the substitution of Zn by Mn ions. The determination of such

Table 4 Listed are: the optical bandgap (E_g), Urbach energy (E_U), the interband oscillating wavelength (λ_o), the refractive index at long-wavelength (n_∞), and the average oscillator strength (S_o) for pure ZnO and Mn-doped ZnO NPs

Samples	E_g (eV)	E_U (eV)	n_∞	λ_o (nm)	$S_o \times 10^{14} \text{ (m}^{-2}\text{)}$
0	3.47	4	8.72	347.59	6.2
0.01	4.01	2.1	3.33	371.58	0.73
0.05	4.57	2.7	3.15	352.88	0.72

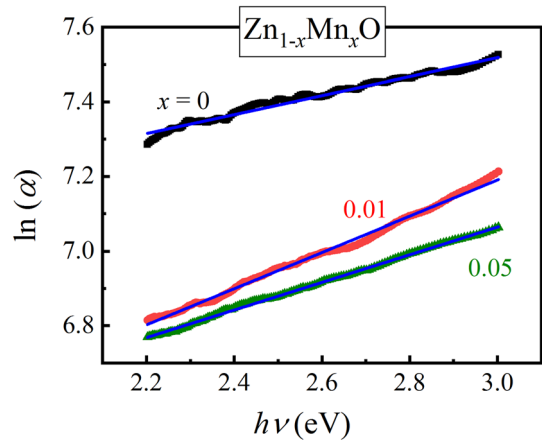


Fig. 12 The plots of $\ln(\alpha)$ against $h\nu$ for $Zn_{1-x}Mn_xO$ NPs, where $x = 0, 0.01$ and 0.05 . The solid blue lines represent the fitting, according to the Urbach relation (Eq. 8) (Color figure online)

parameters contributes to modeling the properties of these materials for use in optical devices.

4 Conclusions

Single-phase $Zn_{1-x}Mn_xO$ samples, where $x = 0, 0.01$ and 0.05 NPs were prepared and characterized. The structure of all studied samples is hexagonal wurtzite. The FE-SEM images showed that the crystal sizes of the samples are almost consistent with those calculated using XRD patterns. The EDX data confirmed the purity of the prepared samples. The results of the FTIR and the values of the average lattice strains gave evidence for the substitution of Zn by Mn ions in the ZnO lattice because of the slight shift of the FTIR peaks in addition to the values of the bond lengths and internal lattice strains.

It was observed that the dielectric permittivity and the ac conductivity of pure ZnO are significantly increased with the doping of Mn ions because of

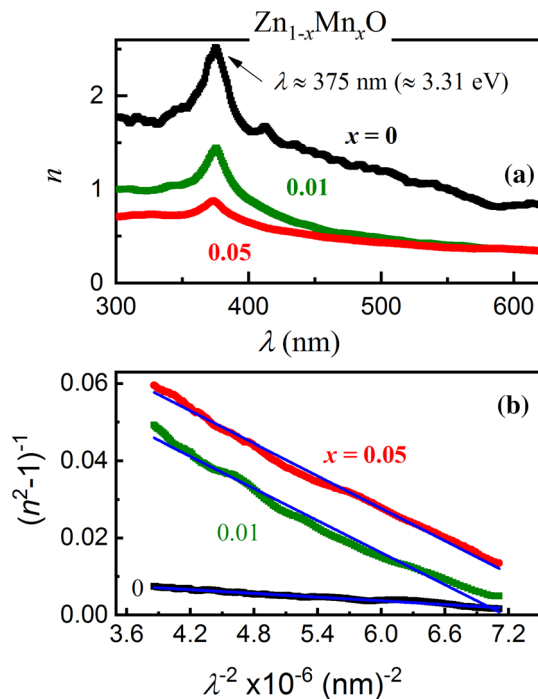


Fig. 13 **a** The dependence of the refractive index (n) on the λ . **b** $(n^2 - 1)^{-1}$ versus λ^{-2} for pure ZnO and Mn-doped ZnO NPs. The solid red lines in (b) are the linear fit of Eq. 10

interfacial polarization. The frequency-dependent ac conductivity was described according to the law that σ_{ac} is proportional to f^s , within the frequency (2–90 kHz) and temperature (333–393 K) ranges. The conduction mechanism can be attributed to small polaron hopping. Besides, the optical absorbance, transmittance, and refractive index of ZnO NPs decreased with substituting Zn by Mn ions in ZnO lattice. The investigated samples exhibited an anomalous dispersion of around 375 nm (≈ 3.31 eV). Different optical parameters of ZnO NPs, such as bandgap transition, Urbach energy, and the average oscillator strength, were given and found that they depend on the level of doping. Because of the different characteristics of the sample of $x = 0.01$, it showed different electrical properties as well as optical parameters compared to those of other samples. Finally, the enhancement of the dielectric properties of Mn-doped ZnO NPs could be important for suitable applications.

Acknowledgements

Many thanks to Dr. A. Hassen, Professor of Materials Science, Physics Department, Faculty of Science,

Fayoum University, 63514 El Fayoum, Egypt, for useful discussions and constant support during the performance of this work. Thanks also to Dr. A. S. Khalil and Mr. Sayed Ragab, Physics Department, Faculty of Science, Fayoum University, for their fast response to finish the FE-SEM images and EDX experiment in time.

References

1. K.J. Chen, T.H. Fang, F.Y. Hung, L.W. Ji, S.J. Chang, S.J. Young, Y.J. Hsiao, *Appl. Surf. Sci.* **254**, 5791 (2008)
2. S. Sharma, A. Tran, O. Nalamasu, P.S. Duta, *J. Electron. Mater.* **6**, 1237 (2006)
3. A. Franco, H.V.S. Pessoni, *Phys. B* **476**, 12 (2015)
4. G. Nam, H. Yoon, B. Kim, D.-Y. Lee, J.S. Kim, J.-Y. Leem, *J. Nanosci. Nanotechnol.* **14**(11), 8544 (2014)
5. X. Han, S. Wahl, P.A. Russo, N. Pinna, *Nanomaterials* **8**, 249 (2018)
6. T.M. Hammad, S. Griesing, M. Wotocek, S. Kuhn, R. Hempelmann, U. Hartmann, J.K. Salem, *Int. J. Nanoparticles* **6**(4), 324 (2013)
7. K.P. Raj, K. Sadaiyandi, A. Kennedy, S. Sagadevan, Z.Z. Chowdhury, M.R.B. Johan, F. Abdul-Aziz, R.F. Rafique, R.T. Selvi, R.R. Bala, *Nanoscale Res. Lett.* **13**, 229 (2018)
8. R.K. Sharma, S. Patel, K.C. Pargaian, *Adv. Nat. Sci. Nanosci. Nanotechnol.* **3**, 035005 (2012)
9. S.A. Sundar, N.J. John, *Int. J. Eng. Appl. Sci. (IJEAS)* **3**(3), 26 (2016)
10. J. Han, M. Shen, W. Cao, A.M.R. Senos, P.Q. Mantas, *Appl. Phys. Lett.* **82**, 67 (2003)
11. S.V. Vegesna, V.J. Bhat, D. Bürger, J. Dellith, I. Skorupa, O.G. Schmidt, H. Schmidt, *Sci. Rep.* **10**, 6698 (2020)
12. X. Yan, D. Hu, H. Li, L. Li, X. Chong, Y. Wang, *Phys. B* **406**, 3956 (2011)
13. S.M. Shah, H. Naz, R.N. Ali, F. Alam, A. Ali, M. Farooq, A. Shah, A. Badshah, M. Siddiq, A. Waseem, *Arab. J. Chem.* **10**, 1118 (2017)
14. M.A. Dar, D. Varshney, *Superlattices Microstruct.* **114**, 340 (2018)
15. R. Viswanatha, S. Sapra, S.S. Gupta, B. Satpati, P.V. Satyam, B.N. Dev, D.D. Sarma, *J. Phys. Chem. B* **108**, 6303 (2004)
16. V. Mote, J. Dargad, B. Dole, *Nanosci. Nanoeng.* **1**(2), 116 (2013)
17. Y.S. Wang, P.J. Thomas, P. O'Brien, *J. Phys. Chem. B* **110**(43), 21413 (2006)
18. J. Han, P.Q. Mantas, A.M.R. Senos, *J. Eur. Ceram. Soc.* **21**, 1883 (2001)

19. W.-D. Zhou, D. Dastan, J. Li, X.-T. Yin, Q. Wang, *Nanomaterials* **10**, 785 (2020)
20. M. Shatnawi, A.M. Alsmadi, I. Bsoul, B. Salameh, M. Mathai, G. Alnawashi, G.M. Alzoubi, F. Al-Dweri, M.S. Bawa'aneh, *Results Phys.* **6**, 1064 (2016)
21. K. Rekha, M. Nirmala, M.G. Nair, A. Anukaliani, *Phys. B* **405**, 3180 (2010)
22. T.A. Abdel-Baset, Y.-W. Fang, B. Anis, C.-G. Duan, M. Abdel-Hafiez, *Mater. Sci. Semicond. Process.* **17**, 162 (2014)
23. G. Srinivasan, R.T. Rajendra Kumar, J. Kumar, *J. Sol Gel Sci. Technol.* **43**, 171 (2007)
24. A.A. Othman, M.A. Osman, E.M.M. Ibrahim, M.A. Ali, A.G. Abd-Elrahim, *Mater. Sci. Eng. B* **219**, 1 (2017)
25. S.N. Danilchenko, O.G. Kukharenko, C. Moseke, I.Y. Prot-senko, L.F. Sukhodub, B. Sulkio-Cleff, *Cryst. Res. Technol.* **37**(11), 1234 (2002)
26. A. Jafari, K. Tahani, D. Dastan, S. Asgary, Z. Shi, X.-T. Yin, W.-D. Zhou, H. Garmestani, Ş Tǎlu, *Surf. Interfaces* **18**, 100463 (2020)
27. M. Kahouli, A. Barhoumi, A. Bouzid, A. Al-Hajry, S. Guermazi, *Superlattices Microstruct.* **85**, 7 (2015)
28. T.M. Hammad, S. Griesing, M. Wotocek, S. Kuhn, R. Hempelmann, U. Hartmann, J.K. Salem, *Appl. Nanosci.* **3**, 153 (2013)
29. M.A.R. Bonifácio, H.L. Liraa, L.S. Neivab, R.H.G.A. Kiminamic, L. Gama, *Mater. Res.* **20**(4), 1044 (2017)
30. Y.-M. Hao, S.-Y. Lou, S.-M. Zhou, R.-J. Yuan, G.-Y. Zhu, N. Li, *Nanoscale Res. Lett.* **7**, 100 (2012)
31. B. Manikandan, T. Endo, S. Kaneko, K.R. Murali, R. John, *J. Mater. Sci. Mater. Electron.* **29**, 9474 (2018)
32. M.F. Khan, A.H. Ansari, M. Hameedullah, E. Ahmad, F.M. Husain, Q. Zia, U. Baig, M.R. Zaheer, M.M. Alam, A.M. Khan, Z.A. AlOthman, I. Ahmad, G.M. Ashraf, G. Aliev, *Sci. Rep.* **6**, 27689 (2016)
33. P. Norouzzadeh, K. Mabhouti, M.M. Golzan, R. Naderali, *J. Mater. Sci. Mater. Electron.* **31**, 7335 (2020)
34. D. Dastan, N. Chaure, M. Kartha, *J. Mater. Sci. Mater. Electron.* **28**, 7784 (2017)
35. G. Srinet, R. Kumar, V. Sajal, *J. Appl. Phys.* **114**, 33912 (2013)
36. P.P. Sharmila, J.T. Nisha, *AIP Conf. Proc.* **1620**, 462 (2014)
37. P.S. Vindhya, T. Jeyasingh, V.T. Kavitha, *AIP Conf. Proc.* **2082**, 080005 (2019)
38. A.M. Saleh, R.D. Gould, A.K. Hassan, *Phys. Status Solidi (a)* **139**(21), 379 (1993)
39. R. Bahri, H.P. Singh, *Thin Solid Films* **62**, 291 (1979)
40. A.K. Roy, K. Prasad, A. Prasad, *Process. Appl. Ceram.* **7**(2), 81 (2013)
41. S.A. Ahmed, *Results Phys.* **7**, 604 (2017)
42. S. Abouelhassan, *Chin. J. Phys.* **48**(5), 650 (2010)
43. G. Srinet, P. Varshney, R. Kumar, V. Sajal, P.K. Kulriya, M. Knobel, S.K. Sharma, *Ceram. Int.* **39**, 6077 (2013)
44. N.F. Mott, E.A. Davis, *Electronic Process in Non-Crystalline Materials*, 2nd edn. (Oxford University Press, Oxford, 1979), p. 273
45. J. Tauc, in *Optical Properties of Solid*. ed. by A. Abeles (North Holland, Amsterdam, 1972), p. 277
46. F. Urbach, *Phys. Rev.* **92**, 1324 (1953)
47. I.S. Yahia, A.A.M. Farag, M. Cavas, F. Yakuphanoglu, *Superlatt. Microstruct.* **53**, 63 (2013)
48. M. Caglar, S. Ilican, Y. Caglar, F. Yakuphanoglu, *Appl. Surf. Sci.* **255**, 4491 (2009)
49. H. Yoshikawa, S. Adachi, *Jpn. J. Appl. Phys.* **36**, 6237 (1997)
50. A.A.M. Faraga, M. Cavas, F. Yakuphanogluc, F.M. Aman-ullahd, *J. Alloys Compd.* **509**, 7900 (2011)
51. J. López, E. Solorio, H.A. Borbon-Nuñez, F.F. Castellón, R. Machorro, N. Nedev, M.H. Fariás, H. Tiznado, *J. Alloys Compd.* **691**, 308 (2017)
52. B.J. Zheng, J.S. Lian, L. Zhao, Q. Jiang, *Appl. Surf. Sci.* **253**, 2910 (2010)

Publisher's Note Springer Nature remains neutral with regard to jurisdictional claims in published maps and institutional affiliations.